Biosourced, highly porous, carbon xerogel microspheres†

L. I. Grishechko,[ab] G. Amaral-Labat,[a] V. Fierro,[a] A. Szczurek,[a] B. N. Kuznetsov[bc] and A. Celzard*[a]

The first tannin-based carbon xerogel microspheres were prepared and characterised. The materials were synthesised by inverse emulsion polymerisation in sunflower oil, based on the same formulation but using two main independent variables: stirring speed and surfactant amount. The resultant sol–gel spheres were then washed, dried in air, and pyrolysed. The effect of stirring speed and surfactant amount on carbon microsphere size distribution and porous texture was investigated in detail. Depending on the cases, ultramicroporous carbon microspheres with extremely narrow pore size distributions centred at 0.4–0.5 nm, zero mesoporosity, negligible macroporosity and median diameters close to 40 μm, could be obtained. These characteristics are typical of expensive commercial carbon molecular sieves, whereas the present materials were prepared with cheap and renewable precursors using a very simple method.

Introduction

Many porous carbon materials produced from countless precursors and through different methods have been reported so far.[1–3] The majority of such materials deals with porous carbons, and activated carbons represent the majority of them, being rather cheap and having many different applications. Carbon gels are another family of porous carbons, having lower surface areas than activated carbons and being more expensive due to the complex process for preparing them. However, the interest in gels lies in their very different porous structure and monolithic aspect, justifying their preparation and their application for niche markets. From the first silica aerogels obtained by Kistler in 1932,[4] this kind of porous material was successfully prepared from various precursors and with different sizes and morphologies. Especially, polymer gels were synthesised, from which organic aerogels, xerogels or cryogels could be derived, depending on the nature of the drying process: supercritical, subcritical or freeze drying, respectively. Most of the time, such materials could be converted into their corresponding carbon counterparts after pyrolysis.

The most widespread and well-known carbon gels are based on resorcinol-formaldehyde resins, which were investigated from the end of the eighties.[5] Later researches paid particular attention to synthesis, structural characteristics and physical properties of derived carbon aerogels, but most of them dealt with a classical scheme based on four steps: sol–gel polymerisation of organic oligomers, solvent exchange, supercritical drying and nally high-temperature carbonisation. The interest for aerogel-type materials is indeed due to the broad range of possibilities and applications they can offer, whether in chemical or electrical engineering because of their high and controllable porosity, good electrical conductivity, corrosion and acid resistance and bio-stability, amongst others. As a consequence, they are promising materials for being used as electrodes of high-power sources, for separation and isolation of heavy metal ions, as chromatographic packing, catalyst supports, thermal insulators, as well as in a variety of other applications for which other porous carbons such as classical activated carbons are less relevant (see ref. 6–8 and references therein).

Therefore, the search for new synthesis routes and new forms of carbon gels is a hot topic. So far, quite a lot of precursors for the fabrication of carbon gels have been reported, such as phenol,[9–11] polyurethane,[12] cresol,[13,14] and other polymers.[15–17] At the present time, natural polymers as precursors of new carbon materials are very topical because of their availability, absence of – or lower – toxicity, renewable character and low cost. Polysaccharides such as cellulose,[18,19] chitin[20] and starch[21,22] were suggested as biomass-derived raw materials for preparing aerogels and their carbon counterparts, but polyphenols such as lignin were also demonstrated to work quite well.[23–25]

In recent years, our group focused on the production of new carbons materials from poorly known polyphenols: condensed flavonoid) tannins. Condensed tannins extracted from Mimosa

barks are commercially available and present constant and reproducible properties, which are rare qualities for a plant-based resource. These compounds are naturally obtained as oligomers presenting different degrees of polymerisation, and can be easily crosslinked further, for example by reaction with formaldehyde[26] or by auto-condensation,[27] thereby leading to infusible and insoluble resins. Condensed tannins from Mimosa bark extracts mainly comprise prorobinetinidin, see Fig. 1(a), which represents about 70% of the total content. The second most abundant flavonoid is profisetinidin, up to 25%,[26] see Fig. 1(b).

We showed that tannins have a great potential as precursors of carbon gels and can indeed easily substitute toxic compounds such as resorcinol or phenol. Carbon gels produced from tannin can have high specific surface area (higher than 1200 m^2 g^{-1}), high porosity (up to 95%), and well-controlled porous structure.[28–30] However, so far, such materials were never obtained with special morphology except that imposed by the geometry of the vessel in which they were prepared, which may be a problem when looking for specific applications. For example, it has been suggested that microspheres of carbon gels, i.e., having both a spherical shape and a small size, might have improved properties in applications such as adsorption,[31–34] catalysis[35] and energy conversion and storage,[36] e.g. as supercapacitor electrodes.[37–39]

Another important application in which porous carbon materials with spherical shape are highly sought-after is gas separation and purification, often based on molecular sieves. Generally speaking, carbon molecular sieves (CMS) are a special class of microporous carbon materials having a specific surface area typically within the range 500–1200 m^2 g^{-1}, and a very narrow distribution of very small pores. The molecular sieve effect is indeed due to the major contribution of pores of width 0.4–1.1 nm. The efficiency of the separation process by the CMS is determined by two main factors: preferential adsorption of one component of the mixture and adsorption rates of individual components, which depend on molecular size and on pore entrance width. From where the great importance of the porous texture of commercial materials such as, for example, Carbosieve® adsorbents, used for the separation of gaseous C_1–C_2 hydrocarbons and C_2–C_5 volatile organic compounds.[40]

Carbon molecular sieves can be prepared from coal,[41–43] wood-based biomass,[44] polymers[40,45–47] and carbon fibres.[48,49] Different methods can be used, depending on the precursor, but the standard one is physical activation.[50–52] Well-known trademarks of carbon molecular sieves include Carbosieve® and Carboxen®.‡ Both are prepared by thermal decomposition of polymers, such as polyvinylidene chloride and Saran.[40] The spherical shape of their individual material give suitable packed beds and these materials are also hydrophobic, allowing them to maintain their performances in high-humidity environments. However, the high cost of Carbosieve® and Carboxen® may hinder their industrial application at large scale.

The aim of the present work was to prepare tannin-based spherical carbon gel microparticles of controlled diameter and porous texture. For that purpose, inverse emulsion polymerisation of an aqueous tannin–formaldehyde solution was carried out in sunflower oil. Instead of preparing aerogels, requiring the costly and long drying step in supercritical CO_2, carbon xerogel microspheres were synthesised, i.e., by simple evaporative drying in room conditions before pyrolysis was carried out at high temperature under inert atmosphere. The effect of synthesis parameters on microsphere particle morphology and size distribution was investigated in detail, as well as their resultant chemical and porous structures.

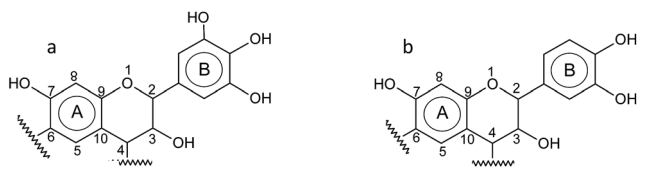

Fig. 1 Main oligomer units in condensed tannins from Mimosa bark extracts: (a) prorobinetinidin (bearing resorcinol A ring and pyrogallol B ring); (b) profisetinidin (bearing resorcinol A ring and catechol B ring)

Experimental

Preparation of carbon xerogel microspheres

Organic xerogel microspheres were first synthesised by inverse emulsion polymerisation of flavonoid tannin with formaldehyde in suflower oil. The tannin used in this work was the commercial Mimosa extract (Acacia mearnsii, de Wild) kindly provided by the company SilvaChimica (St. Michele Mondovi, Italy), and known on the market under the name FINTAN OP. Details about composition, chemical formula, reactivity and impurities have been abundantly given elsewhere.[30,53] Briefly, such commercial Mimosa tannin extract consists of 80–82% of actual phenolic flavonoid materials, whose reactivity with aldehydes is similar to that of resorcinol. Therefore, high-quality thermoset resins, having a high carbon yield around 45% (ref. 54 and 55) can be derived from this natural raw material.

The inverse emulsion polymerisation was carried out as follows. A tannin–formaldehyde (TF) solution was first prepared by dissolving Mimosa tannin (9 g) in distilled water (12.15 g). Stirring was performed for 30 min at room temperature to ensure complete dissolution. Formaldehyde (18 g of 37 wt% aqueous solution) was then added. Although harmful, such chemical was the most efficient one but, when crosslinking tannin, needs to be used in lower proportions than what is required for phenol or resorcinol. The fraction of reactants (sum of tannin + formaldehyde, both on dry basis) in the solution was fixed at 40 wt%. Doing so, the pH was measured and found to be 4.3. In another glass vessel, food-quality sunflower oil was mixed with SPAN 80 (Sigma Aldrich), a commercial sorbitan mono-oleate non-ionic surfactant having an HLB of 4.3. Several volume ratios of surfactant to sunflower oil were tested: 1, 5, and 10 vol%. The homogeneous TF solution was then transferred into a 600 mL round-bottom flask, into which the

surfactant–sunflower oil mixture was also added in such a way that the volume ratio of TF solution to sunflower oil was 1/6. The flask was heated at 80 °C and stirred at different speeds: 200, 500, 800 or 1200 rpm for 1 h, until non-sticky sol–gel spheres were formed. The obtained TF hydrogel microspheres were then separated from sunflower oil by centrifugation and washed with a 5 wt% aqueous solution of liquid (dishwashing) detergent to remove the residual oil. Such commercial detergent contained between 15 and 30 wt% of anionic surfactant.

The microspheres were carefully recovered and soaked in dry ethanol in a closed Erlenmeyer flask. The latter was installed on an orbital shaker and gently stirred at 200 rpm and room temperature for exchanging the water inside the porosity of the microspheres with ethanol. The ethanol was replaced every day by fresh, dry one during 5 days, after which the exchange was assumed to be complete. The resultant alcogel microspheres were left to dry in room temperature and pressure conditions for one week, thus leading to xerogel microspheres. Such tannin-based, organic xerogels were transferred into a quartz boat and heated at 2 °C min^{-1} up to 900 °C in a tubular horizontal furnace continuously flushed by high-purity nitrogen. The set point was maintained during 2 h before the furnace was allowed to cool under nitrogen flow. The resultant carbon xerogel microspheres were termed CXTFsph x/y, where C, X, T, F, sph, x and y stand for carbon, xerogel, tannin, formaldehyde, spheres, stirring speed (rpm) and surfactant/sunflower oil (vol%), respectively.

Carbon microspheres characterisation

Fourier-transform infrared (FTIR) spectroscopy studies were carried out with an IRAffinity 1 spectrometer (Shimadzu, Japan), using organic (i.e., non-pyrolysed) samples (1.5 mg) ground, dispersed in – and pressed with – 200 mg of dry KBr. The pellets were investigated in transmission mode from 400 to 4000 cm^{-1} (20 scans per spectrum at a resolution of 4 cm^{-1}). Chemical differences between raw Mimosa tannin samples and xerogel microspheres were especially looked for.

The pyrolysis behaviour of carbon spheres was performed by thermogravimetry using a NETZSCH STA 449 F3 thermobalance. Thermal stability was investigated by heating the samples from 25 to 900 °C in a flow of pure argon at a maximum heating rate of 10 °C min^{-1}. Bulk elemental analyses of samples were carried out with a CHONS elemental analyser (Vario EL cube, Elementar, Germany) to determine first carbon, hydrogen, nitrogen and sulphur contents by combustion of the samples at about 1700 °C (a temperature induced in a furnace, heated at 1150 °C, by a tin foil wrapping the samples and used as catalyst) in a mixed stream of oxygen and helium, the latter being used as carrier gas. Oxygen was quantified with the same equipment in a second step, using a different procedure and another analytic column.

Finally, Raman spectra of carbonaceous samples without preparation were collected with a Horiba XploRa Raman spectrometer, under a microscope using a 100 objective. The Raman-scattered light was dispersed by a holographic grating with 1200 lines per mm and detected by a CCD camera. A laser of wavelength 532 nm filtered at 10% of its nominal power was used, leading to an incident power lower than 2 mW. The latter allowed short acquisition time and low noise, without any heating or modification of the sample under the beam. Each spectrum was obtained by accumulation of 2 spectra recorded from 800 to 2200 cm^{-1} over 120 s. No tangible differences were observed from one part of the sample to another or from samples to samples. Therefore, only one spectrum was investigated in detail, and was fitted by using five mixed Gaussian–Lorentzian profiles for the bands D_4, D_1, D_3, G and D_2 appearing at increasingly high wavenumbers (see for example ref. 56).

The morphology of the carbon microspheres was observed by scanning electron microscopy (SEM), using a FEI Quanta 600 FEG equipped with a detector of secondary electrons. The distribution of sizes was estimated from SEM pictures through image analysis using ImageJ software. Median, mean, and mode diameters, as well as the standard deviations, were obtained by measurements on a population of at least 700 spheres, according to the method described elsewhere.[57] Median diameters are particle diameters corresponding to 50% accumulation, mean diameters are arithmetic means of the frequency distributions, and mode diameters correspond to the peaks of the frequency distributions.

The packing density, ρ_p (g cm^{-3}), was measured for all carbon xerogel microspheres using a Geopyc 1360 Envelope Density Analyser (Micromeritics, USA), leading to the envelope volume, V_e (cm^3), as an average of five analytical runs. Knowing the mass, m (g), of each sample, the packing density was calculated according to:

$$\rho_p = \frac{m}{V_e} \quad (1)$$

The skeletal density, ρ_s (g cm^{-3}), was estimated with a helium pycnometer Accupyc II 1340 (Micromeritics, USA). For that purpose, samples were finely crushed for avoiding any error related to possibly closed porosity, and were dried in vacuum overnight at 85 °C. From bulk and skeletal densities, the overall porosity of the microsphere packings, Φ (dimensionless), and their specific pore volume, V_{sp} (cm^3 g^{-1}), could be calculated as:

$$\Phi = 1 - \frac{\rho_p}{\rho_s} \quad (2)$$

$$V_{sp} = \frac{1}{\rho_p} - \frac{1}{\rho_s} \quad (3)$$

The porous texture of the samples was characterised by treating nitrogen and carbon dioxide adsorption isotherms obtained at −196 °C and 0 °C, respectively, using automatic adsorption devices ASAP 2020 and ASAP 2420 (Micromeritics, USA), respectively. Before all gas adsorption experiments, the samples were outgassed under secondary vacuum at 270 °C for 48 h. Nitrogen isotherms were used to determine the BET specific surface area, S_{BET} (m^2 g^{-1}), the total pore volume, V_T (cm^3 g^{-1}) obtained at a relative pressure of 0.99, and the micropore volume, V_{DR,N_2} (cm^3 g^{-1}) using the Dubinin–Radushkevich (DR)

formalism. Carbon dioxide isotherms were also used to calculate the micropore volume, V_{DR,CO_2} ($cm^3\ g^{-1}$), with the same DR formalism in order to determine whether existed. Both nitrogen and carbon dioxide isotherms were finally treated with the NLDFT formalism provided by SAIEUS software (Micromeritics) for calculating the pore size distribution, the micropore volume, $V_{m\text{-}NLDFT}$ ($cm^3\ g^{-1}$), and the surface area, S_{NLDFT} ($m^2\ g^{-1}$). The mesopore volume, V_{meso} ($cm^3\ g^{-1}$), was calculated by subtracting $V_{m\text{-}NLDFT}$ to V_T.

In addition to this, mercury porosimetry experiments (AutoPore IV 9500, Micromeritics, USA) were tested. The aim was to determine the macro–mesopore size distributions as well as the macropore volumes, but the impossibility of clearly separating intergranular voids and intraparticle porosity made us renounce to this technique after a few trials only. The materials' macropore volumes were therefore only roughly estimated based on a compacity of 74% for the packing of microspheres. This value corresponds to that of an ordered packing of identical spherical particles. However, given that the microspheres were not monodisperse, see next section, smaller particles were expected to insert between bigger ones, inducing a higher compacity. 74% was therefore considered as a lower bound for estimating the intergranular porosity, V_{inter} ($cm^3\ g^{-1}$), which therefore reads:

$$V_{inter} = \frac{\delta(1 - 0.74)}{r_p} \quad (4)$$

As the total volume of the packing is the sum of different contributions: solid carbon, micropores, mesopores, macropores and intergranular voids, then it is easy to show that the macropore volume, V_{macro} ($cm^3\ g^{-1}$), reads:

$$V_{macro} < \frac{0.74}{r_p} - \frac{1}{r_s} - V_m - V_{meso} \quad (5)$$

In eqn (5), the sign "<" is due the fact that the compacity is expected to be higher than 74%. Mixing two sizes of carbon grain was indeed shown to make the packing density increase by more than 25%.[58] Even if the initial compacity had been chosen equal to that of a random packing of identical spheres, 64%,[59] the true compacity of the blend of different microsphere sizes would therefore likely be close to 80%.

Results and discussion

For chemical studies, not all samples were investigated because all were prepared from the same basic formation. The major differences in the as-obtained microspheres, in terms of particle size and porous structure, were indeed only due to stirring speed and amount of surfactant during inverse emulsion polymerisation, see below. The latter was carried out, as explained in the previous section, in sunflower oil. In order to check that the latter was completely removed after separation and washing steps, the organic xerogel samples were investigated by optical microscopy, IR-spectroscopy and elemental analysis.

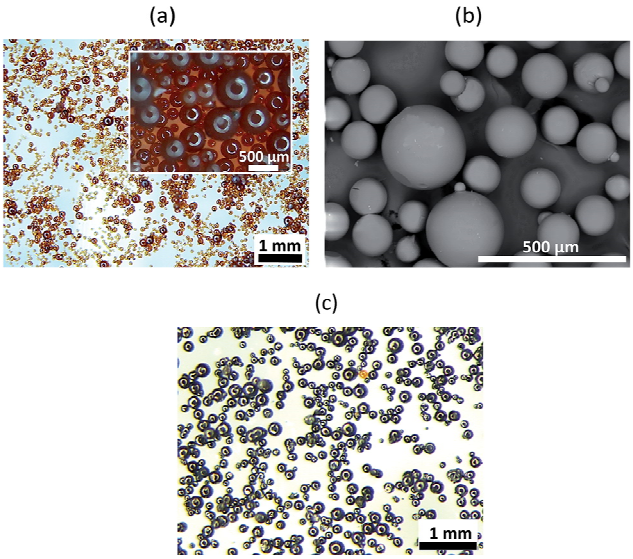

Fig. 2 (a) Optical, and (b) SEM images of tannin–based organic xerogel microspheres prepared at a stirring speed of 200 rpm without surfactant. (c) Optical image of their carbonaceous counterparts.

The obtained organic samples were translucent with a light brown colour and a very even spherical shape, as can be seen in Fig. 2(a). No evidence of sunflower oil could be observed, as all particles were individually separated from each other. Traces of oil indeed were found to produce a strong agglomeration. The xerogel microspheres prepared at a stirring speed of 200 rpm without surfactant were analysed by FTIR-spectroscopy. Fig. 3 shows the corresponding spectrum of the organic xerogel microspheres compared to that of raw Mimosa tannin extract. The IR spectra show that both materials presented the main same peaks but with different intensities. The very broad band within the range 3500–3100 cm^{-1} are attributed to –OH groups, whose amount decreased in the xerogel due to crosslinking of flavonoid units. IR bands in the range 2980–2880 cm^{-1}, attributed to the stretching of CH_2 and CH_3 aliphatic groups, were almost absent in agreement with the molecular structures

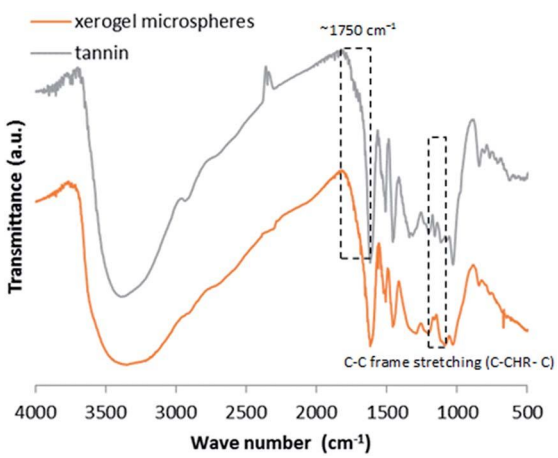

Fig. 3 FTIR spectra of raw Mimosa tannin extract (top) and organic tannin–formaldehyde xerogel microspheres (bottom).

shown in Fig. 1. The presence of a shoulder at 1750 cm^{-1}, corresponding to carbonyl groups and only visible in tannin, can be explained by rearrangement of catechin acid during the extraction process.[60] This shoulder was absent in the spectrum of xerogel microspheres, but an intense peak should have been observed at the same wavenumber if residual sun㳀ower oil was present.[61]

Therefore, it can be assumed that sunflower oil was totally extracted after microspheres washing. Peaks in both tannin and xerogels IR spectra between 1610 and 1450 cm^{-1} are characteristic of aromatic skeletal vibration (–C▌C– aromatic bonds). No peak attributable to sunflower oil expected from its triglyceride content, whether from stretching of carbonyls and –C–O– groups from esters, from in-plane and out-of-plane bending of $(–CH_2–)_n$ chain parts, or from ethylenic –C▌C– groups[61] could be evidenced. These results definitely indicate that sunflower oil was completely removed from organic xerogel spherical particles.

Thermal stability and pyrolysis behaviour of tannin–formaldehyde xerogel microspheres were investigated by thermogravimetric analysis. Fig. S1† shows the TG/DTG thermograms of samples prepared without and with 10 vol% of SPAN 80. The heat treatment of organic xerogels in inert atmosphere led to carbon microspheres with a yield of approximately 50 wt%.

According to Fig. S1,† organic xerogels were quite stable up to about 200 C, a temperature below which only a few wt% of water were lost. Above such temperature, degradation occurred according to three main steps. From 200 to 350 C, a gradual weight loss around 14 wt% of the initial weight was observed, followed by a second one of about 12 or 15 wt% from 350 to 440 C or from 350 to 480 C without or with surfactant, respectively. The main last step, up to 700 C, corresponded to around 5 additional wt% of loss with respect to the initial material. Above 800 C, the weight loss quickly stabilised and was almost negligible.

After pyrolysis, the resultant carbon microspheres fully maintained their spherical shape, as seen in Fig. 2(c). The corresponding carbon texture investigated by Raman spectroscopy was found to be typical of a highly disordered carbon, see Fig. S2.† Two broad bands, often referred to as D and G were indeed observed, but their deconvolution into Gaussian–Lorentzian profiles revealed the existence of various contributions. Five bands were indeed required for a perfect f i tting with nearly zero residues, appearing at 1245, 1355, 1500, 1605 and 1615 cm^{-1}. These bands are known as D_4, D_1, D_3, G and D_2, respectively. D_4 is known to be characteristic of highly disordered carbons, whereas D_3 is also present as a very wide band in poorly crystallised carbons. D_2 is due to double scattering and also associated to defects.[62 and refs. therein] And of course, D_1 is the main defect band and G the graphite band. The I_{D_1}/I_G band intensity ratio, most of the time used as graphitisation indicator, was 1.6 definitely in favour of a poorly organised carbon.

Results of elemental analysis are gathered in Table 1 in terms of wt% of C, H, N and O in Mimosa tannin extract and in both organic and carbon xerogel microspheres prepared without and with 10 vol% of surfactant. Crosslinking of tannin increased the carbon content, which was close to 90% after pyrolysis. The samples prepared with surfactant contained more oxygen, but the difference with surfactant-free materials was not that high.

Morphology and particle size distribution of carbon microspheres were systematically investigated by scanning electron microscopy. Fig. 4 shows SEM pictures of samples prepared at different stirring speeds of 200, 500, 800 and 1200 rpm, all other things being equal, i.e., same concentration of TF solid (40 wt%), non-modified pH (4.3), and without surfactant. The produced CXTFsph particles were all nice rounded spheres

Table 1 Elemental analysis of raw Mimosa tannin extract, organic tannin–formaldehyde xerogel microspheres with or without surfactant, and derived carbon materials[a]

	Content (wt%)				
Material	C	H	N	S	O
Raw tannin extract	53.8	5.4	0.6	0.1	40.1
XTFsph 1200/10	57.8	5.2	0.3	0.03	36.7
XTFsph 500	59.1	5.1	0.3	0.01	35.5
CXTFsph 1200/10	86.2	0.7	0.8	ND	12.4
CXTFsph 500	89.9	0.6	0.9	ND	8.6

[a] ND: non-detected, because below detection limit.

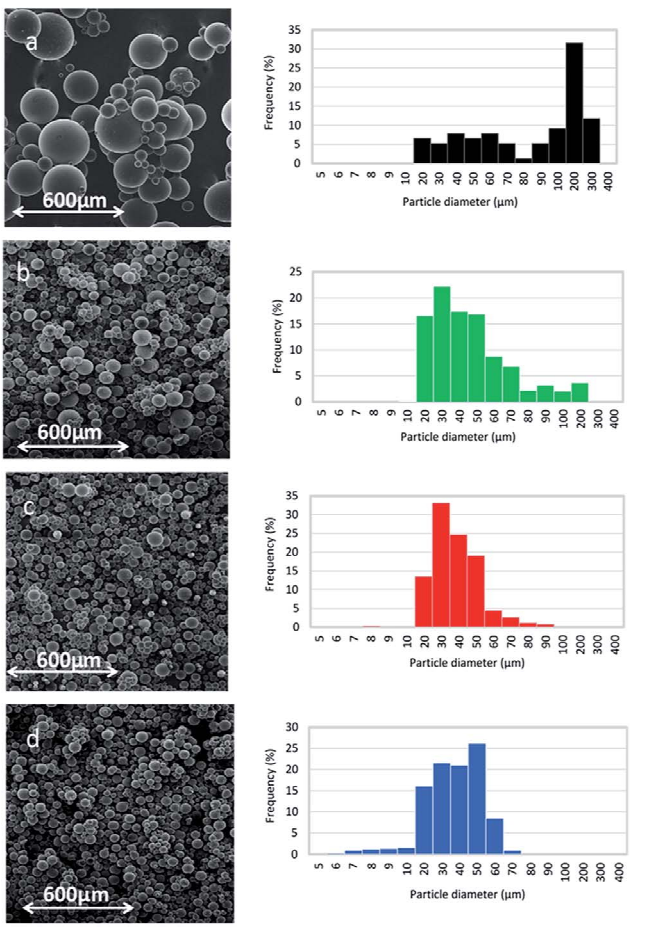

Fig. 4 SEM images and particle diameter distributions of carbon xerogel microspheres prepared without surfactant at different stirring speeds: (a) 200 rpm; (b) 500 rpm; (c) 800 rpm; (d) 1200 rpm.

whose average diameters decreased when the stirring speed increased. The microsphere size distributions derived from many SEM pictures such as those presented in Fig. 4 are also given, and are summarised in Table 2.

Low stirring speeds led to large particles and to broader distributions of sizes, and the gradual increase of stirring speed resulted in smaller and smaller particles. This effect is due to the splitting of TF particles suspended in the oil into smaller ones induced by the increased shear rate in the inverse emulsion. Moreover, no stirring indeed leads to a monolithic gel. The same effect was observed for spherical particles prepared from resorcinol-formaldehyde resin.[37,57] However, in the present case, no significant effect was observed for stirring speeds higher than 500 rpm, as the corresponding diameters remained roughly constant. Stirring can indeed no more efficiently break up TF particles below a critical size, because the induced shear is not high enough for stretching small resin droplets and splitting them further into smaller ones.

The mode diameters of the carbon xerogel particle (i.e., corresponding to the peak values of the distributions), decreased by around 7 times when the stirring speed increased from 200 to 500 rpm or more. Similar trends were observed for median and mean diameters of carbon microspheres. The influence of stirring speed on mean diameters and standard deviations is shown in Fig. 5. As it can be seen, these values decreased when the stirring speed increased.

Not only the stirring speed during polymerisation affected the size of the resultant particles, but the content of surfactant (SPAN 80) in the inverse emulsion also had a strong impact. Fig. 6 indeed shows the influence of the surfactant to sunflower oil ratio on the particle size distribution. Smaller particles were clearly produced at higher amount of surfactant, as their sizes decreased by a factor 2 when the surfactant concentration increased from 1 to 10 vol%. Such effect was expected, as more surfactant indeed promotes higher contact area between oil and water phases and hence smaller resin droplets. Just like for stirring speed, for which no significant effect was observed beyond a given value, the microsphere diameter remained constant above 5 vol% of surfactant, see Fig. 6. Increasing the

Table 2 Characteristic diameters (Ø) of carbon xerogel microspheres

Stirring speed (rpm)	Surfactant content (vol%)	Median Ø (mm)	Mean Ø (mm)	Mode Ø (mm)	Standard deviation (mm)
200	0	100	139	200	105
200	1	50	98	40	102
500	0	40	49	30	35
500	1	40	48	20	33
500	5	20	20	20	9
500	10	20	20	20	6
800	0	40	38	30	14
800	1	30	40	20	32
1200	0	40	37	50	14
1200	1	30	38	20	18
1200	5	20	16	20	7
1200	10	20	16	20	6

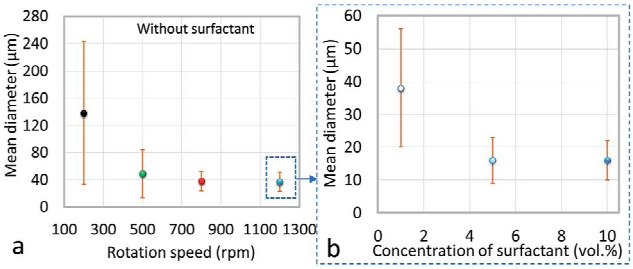

Fig. 5 Influence of: (a) stirring speed, and (b) surfactant content (at same stirring speed of 1200 rpm) during inverse emulsion polymerisation on mean diameters and standard deviations of the resultant carbon xerogel microspheres.

surfactant concentration from 5 to 10 vol% only produced a higher number of spheres in the range 10–20 mm but no shift of the distribution.

The influence of surfactant content during inverse emulsion polymerisation was also shown in Fig. 5(b) for carbon microspheres prepared with the same stirring speed of 1200 rpm. The average diameter did not decrease above 5 vol%, and the standard deviation was slightly reduced in agreement with the aforementioned observations. The same effect was found for

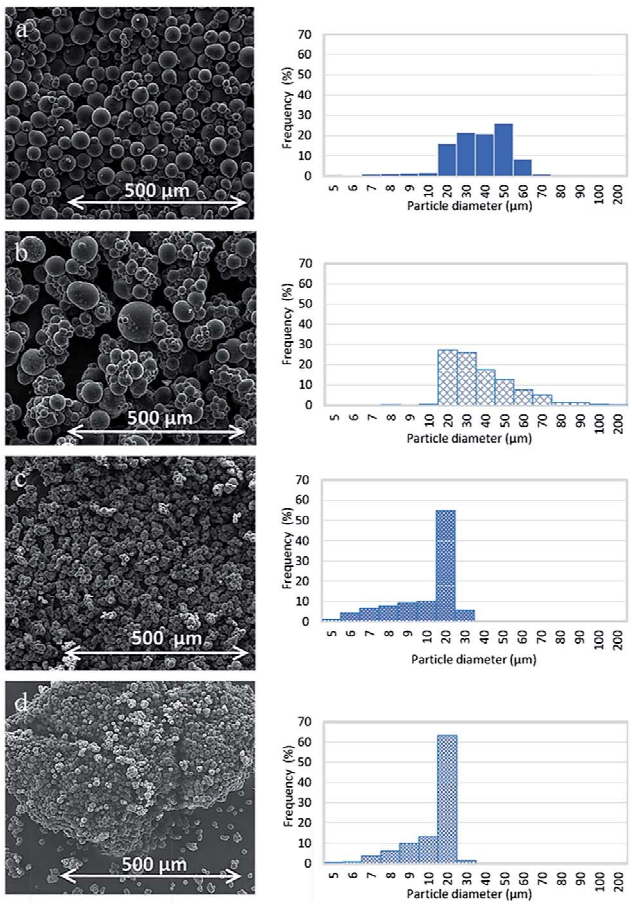

Fig. 6 SEM images and particle diameter distributions of carbon xerogel microspheres prepared at 1200 rpm with different amounts of surfactant: (a) 0 vol%; (b) 1 vol% (c), 5 vol%; (d) 10 vol%.

a stirring speed of 500 rpm, as seen in Table 2. From the above results, it can be concluded that a narrow particle size distribution can be obtained at 5 vol% of surfactant and a stirring speed of 500 rpm during inverse emulsion polymerisation, without the need of increasing these values further.

The content of surfactant also had an influence on the surface morphology of the resultant carbon microspheres, as shown in Fig. S3.† The particles turned from smooth without surfactant (Fig. S3(a)†) to quite rough with apparent pores when prepared with 10 vol% of SPAN 80 (Fig. S3(c)†). This finding is opposite to what has been reported elsewhere,[37] but is in agreement with the higher and coarser porosity observed here at higher surfactant content (see below).

The carbon yield of tannin-based microspheres after pyrolysis at 900 C ranged from 40 to 50%, depending on stirring speed and surfactant amount, see Table 3. These values are close to those of carbon spheres based on resorcinol-formaldehyde resin.[38,57] More surfactant led to a slightly lower carbon yield. This finding is readily explained as follows. Given that the resin was crosslinked in the presence of surfactant, it is very likely that some surfactant remained trapped in the polymer network even after extensive washing steps. As the surfactant is expected to have a far lower carbon yield than that of the phenolic resin, less solid material and more pores were obtained after pyrolysis of xerogel microspheres prepared with higher amounts of surfactant.

The packing density of CXTFsph beds was in the range 0.60–0.98 g cm^{-3}, indicating a significant amount of porosity as the skeletal density measured by helium pycnometry was found to be close to 2 g cm^{-3}, as expected for a disordered carbon prepared at 900 C (see Table 3). The corresponding values of porosity and specific pore volumes calculated by application of eqn (2) and (3), respectively, are also given in Table 3. In most cases, carbon yield decreased and porosity increased when stirring speed and surfactant amount increased.

The pore volumes were significantly lower than those of monolithic aerogels based on tannin–formaldehyde resin.[29] It should indeed be recalled here that the present spheres are xerogels, i.e., were obtained in ambient conditions, and therefore their porosity can never be as high as that of aerogels because of the shrinkage occurring during subcritical drying. But the latter process also has the advantage of being far simpler and cheaper, and also leads to a very narrow porosity as shown below.

N_2 adsorption/desorption and CO_2 adsorption isotherms were analysed, of which typical examples are presented in Fig. S4,† and the main porous texture parameters listed in Table 4 were obtained. Using CO_2 as a probe at 0 C was especially important due to the very narrow porosity of most carbon microspheres and the correspondingly high diffusion resistances, leading to rather high equilibrium time, up to a few hours per data point when using N_2 at _196 C. Micropore volumes measured by CO_2 adsorption, V_{DR,CO_2}, were always higher than those measured with N_2, V_{DR,N_2}, indicating that part of the porosity was not accessible to N_2 due to the higher diffusional resistance at _196 C. Values of S_{BET} of materials prepared at low stirring speed were lower than 10 m^2 g^{-1}, but those prepared at stirring speed higher than 200 rpm were above 500 m^2 g^{-1}. So high values are outstanding for carbon xerogels, i.e., are comparable to those of carbon aerogel[32,57] or cryogel[63] microspheres. Although Fig. 7(a) suggests some correlation between S_{BET} and S_{NLDFT}, the latter was always significantly higher, from 176 to 927 m^2 g^{-1}. This finding is due to the fact that N_2 could not access the narrowest pores, but also to the fact that the BET model is known to underestimate the surface area when very narrow pores exist, in which the formation of a monolayer of nitrogen between two pore walls can occur.

Increasing the amount of surfactant decreased the surface tension of the liquid trapped inside the porosity of the gel, and therefore significantly limited the shrinkage of the gel upon drying. Moreover, adding surfactant to the reaction medium is a well-known method for preparing more porous aerogels and xerogels. As the shrinkage is much lower with surfactant than without surfactant, the pore volumes are higher after drying gels prepared with surfactant. This is especially true for the case of xerogels, i.e., materials submitted to drying in room conditions, and for which very low shrinkages have already been reported.[53,64,65]

As for the effect of stirring speed, the final porosity was controlled again by shrinkage. Although it was not possible to measure the latter, it was observed that the biggest microspheres endured significantly higher shrinkage than smaller ones. As a result, microspheres produced at lower stirring speed

Table 3 Main, overall, characteristics of carbon microspheres: packing density (ρ_p), skeletal density (ρ_s), overall porosity (Φ), specific pore volume (V_{sp}), and carbon yield

Stirring speed (rpm)	Surfactant content (vol%)	ρ_p (g cm^{-3})	ρ_s (g cm^{-3})	Φ (%)	V_{sp} (cm^3 g^{-1})	Carbon yield (%)
200	0	0.98	1.80	45	0.46	48.9
500	0	0.85	1.92	56	0.66	48.2
800	0	0.86	1.97	56	0.66	44.3
1200	0	0.83	1.99	58	0.71	43.8
200	1	0.91	1.96	54	0.59	43.9
500	1	0.63	1.98	68	1.08	41.6
800	1	0.62	1.97	69	1.11	40.1
1200	1	0.66	1.96	66	1.01	40.7
1200	5	0.60	2.01	70	1.17	40.1
1200	10	0.69	2.05	66	0.96	42.3

Table 4 Pore texture parameters of carbon xerogel microspheres

Stirring speed (rpm)	Surfactant content (vol%)	Surface area (m^2 g^{-1})		Pore volume (cm^3 g^{-1})		
		S_{BET}	S_{NLDFT}	V_{DR,N_2}	V_{DR,CO_2}	V_{macro}
200	0	7	176	0.00	0.26	0.00
500	0	617	883	0.23	0.27	<0.08
800	0	574	834	0.22	0.26	<0.09
1200	0	666	927	0.25	0.29	<0.10
200	1	8	60	0.00	0.23	<0.07
500	1	89	190	0.00	0.24	<0.43
800	1	495	685	0.19	0.25	<0.44
1200	1	535	870	0.21	0.25	<0.36
1200	5	571	900	0.25	0.27	<0.47
1200	10	569	934	0.22	0.27	<0.31

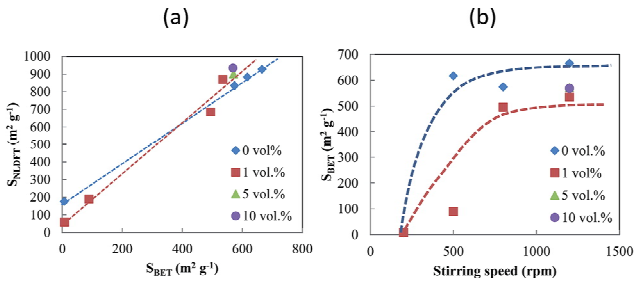

Fig. 7 (a) Comparison between BET and NLDFT surface areas; (b) changes of BET surface area as a function of stirring speed and surfactant content.

(i.e., the biggest ones, see again Fig. 4) presented lower total porosity than those prepared at higher speed, in agreement with the data of Table 3.

Such shrinkage also led to a competition between pore collapse, leading to lower surface areas, and pore narrowing, leading to the opposite result. At low stirring speed, the shrinkage was high so that pore collapse prevailed, hence the low S_{BET} see in Fig. 7(b). At high stirring speed, the shrinkage was low so that pore narrowing prevailed, hence the higher S_{BET}. It is indeed interesting to observe that the surface area varied in an opposite way as that of the microsphere diameter, see again Fig. 5.

When 1 vol% of surfactant was present, S_{BET} unambiguously increased with stirring speed, see Fig. 7(b). The higher shrinkage of bigger spheres obtained at lower stirring speed, producing a more significant pore collapse, may explain their much lower surface area. However, the S_{BET} values of materials prepared with 1 vol% of SPAN 80 were lower than those in the absence of surfactant. When surfactant was present, no significant differences of S_{BET} were observed with different amounts: 1, 5 or 10 vol%, see again Fig. 7(a), but S_{NLDFT} increased from 870 to 934 m^2 g^{-1} when the surfactant content increased from 1 to 10% at 1200 rpm. Mesoporosity was only detected for samples prepared at 1200 rpm and surfactant content ≤5 vol%, but the value of V_{meso} was very low: 0.02 cm^3 g^{-1}. The most important impact of the surfactant was on the macroporosity. No or negligible macroporosity was found in the absence of surfactant, but all samples prepared at stirring speed ≤500 rpm induced macropores volumes in the range 0.3–0.5 cm^3 g^{-1}.

The impact of stirring speed on the pore size distributions, in the absence of surfactant, can be observed in Fig. 8(a). A highly uniform microporous character was evidenced for these materials, with a peak centred on 0.5 nm, except the one prepared at 200 rpm which was almost non-porous with respect to N_2, the latter not being able to penetrate so narrow pores. Low stirring speed, 200 rpm, indeed produced a very narrow micropore size distribution with a peak centred on 0.4 nm. The observed difference of surface area of CXTFsph spherical particles obtained without surfactant at stirring speeds ≤500 rpm was therefore only due to different amounts of identical pores. The CO_2 adsorbed volume, see again Table 4, was always higher than that measured with N_2, confirming the very small sizes of the micropores. On average, V_{DR,CO_2} increased with stirring speed and surfactant content. These trends are more clearly seen when considering the NLDFT surface area in Table 4, more representative of so narrow microporosity. At 1200 rpm, adding increasingly high amounts of surfactant developed the mesoporosity very slightly, see again Table 4. Such f i nding is hardly noticed in the mesopore range of the pore size distribution shown in Fig. 8(b). In the same time, the position of the main micropore peak changed a little when the amount of surfactant increased. It is still unclear, although perfectly repeatable, why the material with 5 vol% of surfactant was the only one presenting slightly broader micropores than the others. All the aforementioned findings are the consequences of a subtle

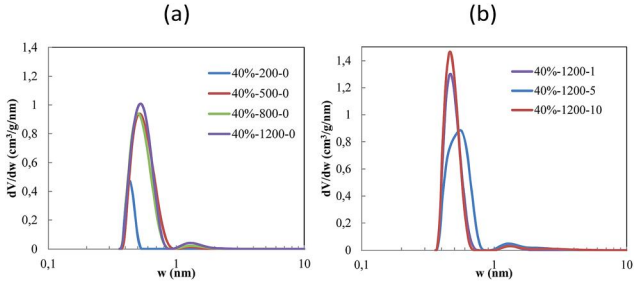

Fig. 8 Pore size distributions of carbon microspheres prepared: (a) without surfactant at different stirring speeds; (b) at the same stirring speed of 1200 rpm with different amounts of surfactant.

balance between pore collapse and pore narrowing induced by the different shrinkages resulting from different stirring speeds and different amounts of surfactant.

CXTFsph carbon microspheres were predominantly microporous with different amounts of macroporosity, depending on the presence of surfactant. Values of mesopore volume were indeed extremely low, not higher than 0.02 cm^3 g^{-1} and even non-measurable in most cases. The macropore volumes (V_{macro}) estimated from eqn (5) are presented in Table 4 and were found to range from 0 to less than 0.5 cm^3 g^{-1}. Mercury porosimetry analysis was carried out on sample CXTF 1200/10 for confirming this order of magnitude. Since mercury at 414 MPa is not able to probe pores narrower than 3.6 nm, and as the mesopore volumes reported in Table 4 were negligible, only macroporosity could indeed be evidenced with this technique.

The raw intrusion curve and the corresponding pore-size distribution are shown in Fig. S5(a) and S5(b),† respectively. Fig. S5(b)† was calculated by application of Washburn's equation to the data of Fig. S5(a),† and reads:

$$D = -\frac{4\gamma \cos\theta}{P} \quad (6)$$

where D (nm) is the pore diameter, and P (MPa), γ (485 mJ m^{-2}) and θ (140°) are the isostatic pressure, surface tension and contact angle of mercury, respectively.

A first pseudo-plateau ending at an intrusion pressure of 0.1 MPa was observed, at which about 0.4 cm^3 g^{-1} of mercury were intruded in the sample, most likely in its intergranular porosity. This value is indeed very close to that predicted by eqn (4), i.e., >0.38 cm^3 g^{-1}. The macropore volume for this sample could therefore be estimated as the difference between such pseudo-plateau and the final intrusion plateau, i.e., 0.8 − 0.4 = 0.4 cm^3 g^{-1}. The latter value is again close to that reported in Table 4, i.e., <0.31 cm^3 g^{-1}. Such comparison, however, can never be very accurate as Fig. S5(b)† shows that the peak of the distribution was centred on 3.5 mm, indicating the intrusion of either large pores such as those already observed in Fig. S3(a) and S3(c),† or interparticle voids, or both.

From the above results, part of the CXTFsph carbon xerogels can therefore be considered as rather well monodispersed carbon microspheres presenting a very narrow microporosity, and especially in the range of ultramicroporosity (0.4–0.5 nm). Such kind of materials is generally used for purification and separation of gases. And indeed, the porous structure of CXTFsph carbon xerogels can be directly compared to that of carbon molecular sieves reported recently[47] or of actual commercial carbon molecular sieves from the Carbosieve® family.§[66,67] The pore size distributions of such molecular sieves are indeed typically centred on 0.5–0.8 nm and present a very low mesoporosity. The same adsorption properties are therefore to be expected for CXTFsph materials.

Conclusion

Carbon xerogel microspheres were prepared for the first time from an aqueous tannin-based solution by inverse emulsion polymerisation in sunflower oil, followed by subcritical drying in room conditions and high-temperature pyrolysis under a nitrogen atmosphere. As expected from the nature of the precursor resin, a highly disordered carbon texture was obtained. The influence on microsphere size and porous structure of both stirring speed and amount of surfactant during the polymerisation process was investigated in detail.

The peaks of the microsphere size distribution could be shifted from 200 to 20 mm. The higher was the stirring speed, the lower was the average size, and/or the higher was the number of small particles beyond a critical speed, above which the distributions were no more shifted. Higher amounts of surfactants also produced smaller microspheres, although again no significant effect was observed above a given value.

The highest BET surface area, about 660 m^2 g^{-1}, was obtained for the materials prepared at the highest stirring speed without surfactant. However, the highest NLDFT surface areas, up to 870 m^2 g^{-1}, were obtained for the materials prepared again at the highest stirring speed but with the highest amount of surfactant. These findings are consistent with the extremely narrow pores present in these carbon xerogels, also having a very narrow distribution of micropore sizes centred on 0.4–0.5 nm. Although macroporosity was present in some cases, the mesopore volumes were almost negligible and therefore the materials were almost purely ultramicroporous.

Their extremely narrow micropore size distribution, associated with the use of a cheap precursor and an inexpensive process, suggests that these new carbon xerogels microspheres may have applications as cost-effective carbon molecular sieves. Given the similarity of porous texture with those of some commercial carbon molecular sieves, their use in GC columns for analysing mixtures of permanent gases and C_1–C_2 hydrocarbons should be considered in priority. Such investigations will be carried out in the near future.

Acknowledgements

The authors gratefully acknowledge the financial support of the CPER 2007–2013 "Structuration du Pôle de Compétitivité Fibres Grand'Est" (Competitiveness Fibre Cluster), through local (Conseil Général des Vosges), regional (Région Lorraine), national (DRRT and FNADT) and European (FEDER) funds. We also thank the Région Lorraine, especially one of us (L.I.G) for her grant through the Lorraine-Russia ARCUS cooperation program.

References

1 M.-M. Titirici, R. J. White, N. Brun, V. L. Budarin, D. S. Su, F. del Monte, J. H. Clark and M. J. MacLachlan, Chem. Soc. Rev., 2014, 44, 250.
2 I. Michio, Q. Jieshan and G. Quangui, Carbon, 2015, 87, 128.
3 A. D. Amit, D. M. Sabelo and J. C. Neil, Mater. Sci. Eng., R, 2010, 70, 1.

4 M. A. Aegerter, N. Leventis and M. M. Koebel, Aerogels Handbook, Springer-Verlag Inc, New York, 2011.
5 R. Pekala and F. Kong, A Synthetic Route to Organic Aerogels – Mechanism, Structure, and Properties, in Proceedings of the 2nd International Symposium on Aerogels (ISA 2) – Journal de Physique Colloques, 1989.
6 A. Celzard, V. Fierro and G. Amaral-Labat, Adsorption by Carbon Gels, in Adsorption by Carbons, Elsevier, 2012, p. 207.
7 N. Job, B. Heinrichs, S. Lambert, J. Pirard, J. Colomer, B. Vertruyen and J. Marien, AIChE J., 2006, 52(8), 2663.
8 C. A. Páez, M. S. Contreras, A. Léonard, S. Blacher, C. G. Olivera-Fuentes, J.-P. Pirard and N. Job, Adsorption, 2012, 18(3–4), 199.
9 D. Wu and R. Fu, Microporous Mesoporous Mater., 2006, 96, 115.
10 D. Wu, R. Fu, Z. Sun and Z. Yu, J. Non-Cryst. Solids, 2005, 351(10–11), 915.
11 G. Amaral-Labat, A. Szczurek, V. Fierro, A. Pizzi, E. Masson and A. Celzard, Microporous Mesoporous Mater., 2012, 158, 272.
12 G. Biesmans, A. Mertens, L. Duffours, T. Woignier and J. Phalippou, J. Non-Cryst. Solids, 1998, 225, 64.
13 Y. Zhu, H. Hu, W. Li and H. Zhao, J. Non-Cryst. Solids, 2006, 352, 3358.
14 W.-C. Lia, A.-H. L. Lub and S.-C. Guoa, Carbon, 2001, 39, 1989.
15 J. Yamashita, T. Ojima, M. Shioya, H. Hatori and Y. Yamada, Carbon, 2003, 41, 285.
16 F. Perez-Caballero, A.-L. Peikolainen, M. Uibu, R. Kuusik, O. Volobujeva and M. Koel, Microporous Mesoporous Mater., 2008, 108, 230.
17 X. Zenga, D. Wu, R. Fu, H. Lai and J. Fu, Electrochim. Acta, 2008, 53, 5711.
18 B. Grzyb, C. Hildenbrand, S. Berthon-Fabry, D. Bégin, N. Job, A. Rigacci and P. Achard, Carbon, 2010, 48, 2297.
19 F. Fischer, A. Rigacci, R. Pirard, S. Berthon-Fabry and P. Achard, Polymer, 2006, 47(22), 7636.
20 C. Tsioptsias, C. Michailof, G. Stauropoulos and C. Panayiotou, Carbohydr. Polym., 2009, 76, 535.
21 X. Chang, D. Chen and X. Jiao, Polymer, 2010, 51, 3801.
22 M. Bakierska, M. Molenda, D. Majda and R. Dziemb, Procedia Eng., 2014, 98, 14.
23 L. Grishechko, G. Amaral-Labat, A. Szczurek, V. Fierro, B. Kuznetsov, A. Pizzi and A. Celzard, Ind. Crops Prod., 2013, 41, 347.
24 F. Chen and J. Li, Adv. Mater. Res., 2010, 113–116, 1837.
25 M. Nishida, Y. Uraki and Y. Sano, Bioresour. Technol., 2003, 88(1), 81.
26 A. Pizzi, Wood adhesive chemistry and technology, Dekker, New York, 1st edn, 1983.
27 N. Meikleham and A. Pizzi, J. Appl. Polym. Sci., 1994, 53, 1547.
28 G. Amaral-Labat, A. Szczurek, V. Fierro and A. Celzard, Mater. Chem. Phys., 2015, 149–150, 193.
29 A. Szczurek, G. Amaral-Labat, V. Fierro, A. Pizzi, E. Masson and A. Celzard, Carbon, 2011, 49(8), 2773.
30 G. Amaral-Labat, A. Szczurek, V. Fierro, N. Stein, C. Boulanger, A. Pizzi and A. Celzard, Biomass Bioenergy, 2012, 39, 274.
31 A. J. Romero-Anaya, M. A. Lillo-Rodenas and A. Linares-Solano, Carbon, 2014, 77, 616.
32 J. Chaichanawong, K. Kongcharoen and S. Areerat, Adv. Powder Technol., 2013, 24(5), 891.
33 S. Ronka, J. Anal. Appl. Pyrolysis, 2014, 110, 390.
34 J. Choma, W. Fahrenholz, D. Jamiola, J. Ludwinowicz and J. Mietek, Microporous Mesoporous Mater., 2014, 185, 197.
35 C. Jianglai, W. Yong, T. Chao, S. Yongjia, R. Lianbing and J. Biwang, Chem. Eng. J., 2014, 242, 285.
36 X. Jiang, X. Ju and M. Huang, J. Alloys Compd., 2011, 509, S864.
37 X. Wang, X. Wang, L. Liu, L. Bai, H. An, L. Zheng and L. Yi, J. Non-Cryst. Solids, 2011, 357, 793.
38 N. Liu, S. Zhang, R. Fu, M. S. Dresselhaus and G. Drsselhaus, Carbon, 2006, 44, 2430.
39 Y. Fan, X. Yang, P.-F. Liu and H.-T. Lu, J. Power Sources, 2014, 268, 584.
40 H. C. Foley, Microporous Mater., 1995, 4, 407.
41 A. A. Lizzio and M. Rostam-Abadi, Fuel Process. Technol., 1993, 34, 97.
42 H. Jiintgen, K. Knoblauch and K. Harder, Fuel, 1981, 60, 817.
43 S. N. Vyas, S. R. Patwardhan, S. Vijayalakshmi and B. Gangadhar, Fuel, 1993, 72(4), 551.
44 A. R. Mohamed, M. Mohannadi and G. N. Darzi, Renewable Sustainable Energy Rev., 2010, 14, 1591.
45 A. Silvestre-Albero, A. Wahby, J. Silvestre-Albero, F. Rodríguez-Reinoso and W. Betz, Ind. Eng. Chem. Res., 2009, 48, 7125.
46 J. Liu, C. Han, M. McAdon, J. Goss and K. Andrews, Microporous Mesoporous Mater., 2015, 206, 207.
47 J. Liu, Y. Liu, D. K. Talay, E. Calverley, M. Brayden and M. Martinez, Carbon, 2015, 85, 201.
48 M. Bikshapathi, A. Sharma, A. Sharma and N. Verma, Chem. Eng. Res. Des., 2011, 89, 1737.
49 T. Orfanoudakia, G. Skodrasb, I. Doliosb and G. P. Sakellaropoulos, Fuel, 2003, 82, 2045.
50 J. Hayashi, Carbon, 1999, 37, 524.
51 K. Miura, J. Hayashi and K. Hashimoto, Carbon, 1999, 29, 653.
52 D. Lozano-Castello, J. Alcaniz-Monge, D. Cazorla-Amoros, A. Linares-Solano, W. Zhu, F. Kapteijn and J. A. Moulijn, Carbon, 2005, 43, 1643.
53 G. Amaral-Labat, L. I. Grishechko, V. Fierro, B. N. Kuznetsov, A. Pizzi and A. Celzard, Biomass Bioenergy, 2013, 56, 437.
54 G. Tondi, V. Fierro, A. Pizzi and A. Celzard, Carbon, 2009, 47, 1480.
55 A. Amaral-Labat, M. Sahimi, A. Pizzi, V. Fierro and A. Celzard, Phys. Rev. E: Stat., Nonlinear, So鋅 Matter Phys., 2013, 87, 032156.
56 M. Pawlyta, J. N. Rouzaud and S. Duber, Carbon, 2015, 84, 479.
57 T. Horikawa, J. Hayashi and K. Muroyama, Carbon, 2004, 42, 169.

58 A. Celzard, A. Albiniak, M. Jasienko-Halat, J. F. Marêché and G. Furdin, Carbon, 2005, 43, 1990.
59 C. Song, P. Wang and H. A. Makse, Nature, 2008, 453(7195), 629.
60 L. Pinga, A. Pizzi, Z. Ding Guo and N. Brosse, Ind. Crops Prod., 2012, 40, 13.
61 A. Rohmana, S. Riyanto, A. M. Sasi and F. M. Yusof, Food Biosci., 2014, 7, 64.
62 D. S. Knight and W. B. White, J. Mater. Res., 1989, 4, 385.
63 T. Yamamoto, T. Ohmori and Y. H. Kim, Microporous Mesoporous Mater., 2008, 112, 211.
64 Y. J. Lee, J. C. Jung, J. Yi, S. H. Baeck, J. R. Yoon and I. K. Song, Current Applied Physics, 2010, 10, 682.
65 J. Li, X. Wang, Q. Huang, S. Gamboa and P. J. Sebastian, J. Power Sources, 2006, 158, 784.
66 R. Noel, J. Busto, S. Schaefer, A. Celzard and V. Fierro, AIP Conf. Proc., 2015, 167, 070001.
67 S. K. Bhatia, Accessibility of Gases and Liquids in Carbons, in Novel Carbon Adsorbents, ed. J. M. D. Tascon, Elsevier, Oxford, 2012, p. 48.